An Experimental Investigation of the Transient Characteristics on a Flat-Plate Heat Pipe During Startup and Shutdown Operations

Y. Wang

K. Vafai
Professor, Fellow ASME

Department of Mechanical Engineering,
The Ohio State University,
Columbus, OH 43210-1107

This work presents an experimental investigation of the thermal performance of a flat-plate heat pipe during startup and shutdown operations. Using the analytical model developed in a previously study, analytical and experimental results on the effect of input power and cooling heat transfer coefficient on the thermal performance of the heat pipe are presented and discussed. The results indicate that the wick in the evaporator section provides the largest resistance to the heat transfer process followed by the wick in the condenser section. It is found that the heat transfer coefficient has an insignificant effect on the maximum temperature difference across the heat pipe where this difference refers to the maximum difference on the outside surfaces of the flat-plate heat pipe. However, as expected, the input heat flux has a substantial effect on the temperature rise where the temperature rise refers to the temperature increase on the outside surface of the heat pipe. It is found that the temperature difference across the heat pipe depends mainly on the input power. The heat transfer coefficient strongly affects the time it takes to reach steady state while input power has a substantially smaller effect. Empirical correlations for the maximum temperature rise, the maximum temperature difference and the time constants are obtained. The experimental results are compared with the analytical results and are found to be in very good agreement. [S0022-1481(00)01803-X]

Keywords: Experimental, Heat Pipes, Heat Transfer, Modeling, Transient.

1 Introduction

The flat-plate heat pipe finds numerous applications such as in electronics cooling and spacecraft radiator segments (Chi [1] and Peterson [2]). The flat-shaped heat pipe also finds applications for very localized heat dissipation where it is difficult to effectively utilize a conventional cylindrical heat pipe due to the limited heat source and sink areas. However, the research work on heat pipes has been mainly focused on the traditional cylindrical heat pipe for a wide variety of applications, and there is far less work conducted on the flat-plate heat pipe. In earlier studies by Vafai and his co-workers, both analytical and numerical investigations were conducted for the vapor and fluid flows as well as for the heat transfer characteristics for the startup process of a flat-plate heat pipe. Vafai and Wang [3] investigated the overall performance of an asymmetrical rectangular flat-plate heat pipe. They developed a pseudo-three-dimensional analytical model for steady incompressible vapor flow in the flat-plate heat pipe. Detailed physics of the transport processes within the heat pipe were analyzed and established. Zhu and Vafai [4] conducted a three-dimensional analytical and numerical study for the steady incompressible vapor and liquid flow in an asymmetrical flat-plate heat pipe. Their results demonstrated that the vapor velocity profile is nonsimilar and asymmetrical and that the transverse pressure variations are small. Later, Zhu and Vafai [5] developed an analytical model to predict the transient thermal behavior of asymmetrical flat-plate heat pipes during the startup process. The temperature distributions within the heat pipe walls and liquid-saturated wicks were obtained analytically. Wang and Vafai [6] developed an analytical model for predicting the thermal performance of flat-plate heat pipes for startup and shutdown operations. The effects of input power and heat transfer coefficient on the performance of the flat-plate heat pipe were investigated.

There is a very limited number of experimental investigations available on flat-plate heat pipes. Furthermore, these few investigations reported system-specific applications and testing data for the flat-plate heat pipes. In addition, the heat pipes utilized in these experiments were based on a simpler structure than those proposed and analyzed by Vafai et al. Among the very few experimental investigations in this area, the works of Kikuchi et al. [7], Basiulis et al. [8], and Thomson et al. [9] can be cited. Kikuchi et al. [7] had carried out experiments on an electrohydrodynamic flat-plate heat pipe. The heat pipe was 100 cm in length and 10 cm in width, and employed three electrodes. The orientation of the heat pipe was horizontal in their study and Freon 11 and 113 were separately used as working fluids. It was found that Freon 11 was superior to Freon 113 from the point of view of thermal transport. Heat transport capabilities up to 150W were recorded. Basiulis et al. [8] conducted experiments to test the performance of flat-plate heat pipes for cooling printed wiring boards. A maximum power input up to 100 W and heat fluxes up to 2 W/cm^2 were reported for the tested heat pipes. Thomson et al. [9] performed experiments to investigate the application of flat-plate heat pipes in cooling of high-power amplifiers (HPA) for communication satellites. The surface temperatures of the heat pipe were measured for three different input powers. In the above studies, no vertical wicks were reported and the condensate return path was not specified. Additional works dealing with some restricted aspects of flat-plate heat pipes can be found in Refs. [10–16]. Once again, it should be noted that the heat pipes utilized in these works were substantially simpler in form than that analyzed by Vafai et al. [4,6,17]. A more recent investigation of the thermal performance of a flat plate heat pipe is given in Wang and Vafai [18].

In this work, an experimental and analytical investigation is

Contributed by the Heat Transfer Division for publication in the JOURNAL OF HEAT TRANSFER. Manuscript received by the Heat Transfer Division, July 3, 1999; revision received, Feb. 23, 2000. Associate Technical Editor: D. Poulikakos.

conducted to characterize the thermal performance of a flat-plate heat pipe. The effects of input heat flux and heat transfer coefficient on the thermal performance of a flat-plate heat pipe are investigated experimentally. The temperature and heat flux distributions as well as empirical correlations for the maximum temperature rise, the maximum temperature difference within the heat pipe, and time constants are presented. The experimental results are compared with the analytical results by Wang and Vafai [6].

2 Analytical Modeling

The analytical model for startup and shutdown operations developed in Wang and Vafai [6] was utilized to predict the performance of the experimental heat pipe. A summary description of the essential parts of the analytical modeling is given below.

The main assumptions for the analysis for the flat plate heat pipe are (1) the heat transfer in the wick is by conduction, (2) the temperature in the vapor phase is uniform at any given time, (3) the thermal properties of the heat pipe wall and the wick are taken to be constant, and (4) heat transfer along the top heat pipe wall and wick in the longitudinal direction is small and is neglected.

For a startup operation, the heat transfer process in the heat pipe is divided into five regimes. The first regime starts when power is turned on and ends when the thermal front reaches the wall-wick interface of the evaporator section. Following this period is the second regime, which starts when the thermal front resumes from the wall-wick interface and ends when the thermal front reaches the wick-vapor interface of evaporator section. In the third regime, the thermal front resumes from the wick-vapor interface and reaches the wick-wall interface of the condenser section. The fourth regime starts when the thermal front progresses from the wick-wall interface and ends when the thermal front reaches the outside wall surface of condenser section. In the fifth and final regime, the outside wall surface of the condenser section begins to increase. For the shutdown operation, the input power is zero and there is only one regime. During this regime, the heat pipe temperatures in all heat pipe walls and wicks decrease with time.

For each period, the temperature distributions in the heat pipe walls and wicks along the normal direction are presented using second-order formulations, which are functions of time. Based on separate energy balance for heat pipe walls and wicks and interface energy and temperature balance at the wall-wick and wick-vapor interfaces, detailed analytical models are developed for each regime in the startup operation. For a shutdown operation, similar procedure was utilized and a separate model is obtained. The derived models consist of close systems of equations, which can be solved numerically.

In the simulation, the temperature distribution within the heat pipe at the end of the startup operation is taken as the initial temperature distribution for the shutdown operation. In this work, the steady-state conditions are assumed to have been reached if the relative deviation between the input and output power is less than 0.2 percent. Similarly, during the shutdown operation, it is assumed that the heat pipe reaches its original temperature if the temperature rise at the outside wall surface of the evaporator section is less than 0.3°C ([6]).

3 Experimental Setup and Procedure

Figure 1 is a schematic of the flat-plate heat pipe. The heat pipe was 190.50 mm in length, 139.70 mm in width, and 34.93 mm in height. The working fluid for the heat pipe was water. The heat pipe walls were made of copper plate, 3.175 mm thick. Attached to the inner surfaces of the heat pipe wall are porous wicks, as shown in Fig. 1. In addition, vertical wicks are used to provide a secondary return mechanism for the condensate. The vapor region is composed of four identical channels. The wicks were composed of sintered copper powder with a thickness of 1.651 mm. The pore radius of the wicks was 3.1×10^{-5} m and their porosity was 50 percent. The permeability of the wicks was 7×10^{-12} m^2. A flexible heater (139.7 mm in length and 50.8 mm in width), specially

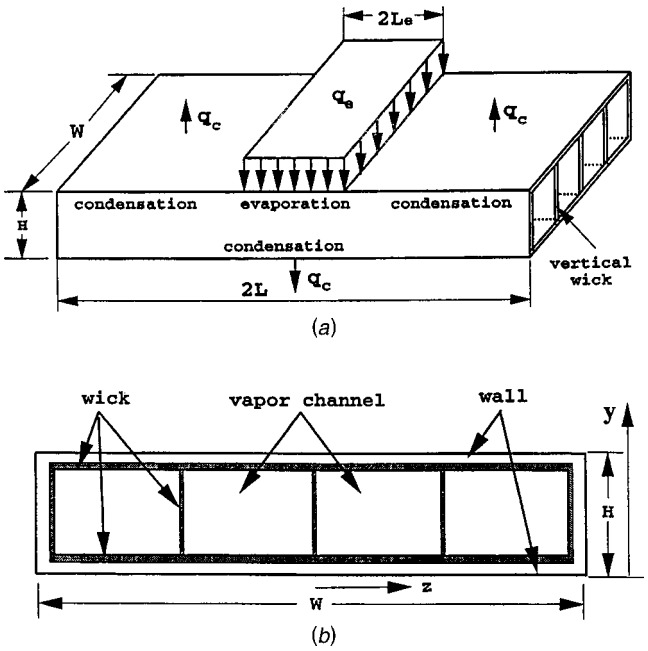

Fig. 1 Schematic of the flat-plate heat pipe: (*a*) geometry of the heat pipe, (*b*) cross-sectional view of the heat pipe

designed for this experiment (Watlow Company, Inc.), was attached along the centerline of the top surface of the heat pipe. The exposed side of the heater was insulated. The heat pipe can be divided into four sections, i.e., one evaporator section on the top center, two smaller identical condenser sections on the top, located on either side of the evaporator section, and a larger condenser section on the bottom (Fig. 1).

Figure 2 is a schematic of the experimental setup. The heat pipe was oriented horizontally in the experiment. A Lexan frame, 34.93 mm in thickness, was constructed to house the heat pipe. The function of the Lexan frame was threefold: (1) to support the heat pipe, (2) to reduce the heat loss through the four edges of the heat pipe, and (3) to insure uniformity of gap thickness around the heat pipe. Taking into account thermal expansion, the inner dimensions of the frame are made larger than the outside dimension of the heat pipe, and a flexible insulation material 2 mm in thickness was installed between the Lexan frame and the heat pipe. The flexible insulation material allows the heat pipe to expand at elevated temperatures. The flexible insulation material also reduces the heat loss through the four edges of the heat pipe.

A channel was designed to house the frame. The cross section of the channel was rectangular (Fig. 2*b*) and its inner dimensions were 217 mm in width, and 45 mm in height. The length of the channel was 540 mm. The frame enclosing the heat pipe was securely mounted within the chamber.

The center part of the top wall of the channel was detachable. The thermocouple wires and the power cord were fed through the detachable top wall; therefore the thermocouple wires and the power cord caused a minimal disturbance on the fluid flow through the channel. In order to seal the top detachable plate, another Lexan plate as well as a gasket were used as shown in Fig. 2(*b*). To insure uniform channel height for each of the three channels, identical spacers were constructed for each section as shown in Fig. 2. This design produces three channels for the water flow as shown in Fig. 2(*b*).

Cooling water enters the water tank through the water supply as shown in Fig. 2(*a*). The water pressure and flow rate were stabilized by the water tank. The cooling water enters the test section, which houses the heat pipe frame and the heat pipe. The flow rate was measured with two float flow meters with different flow rate

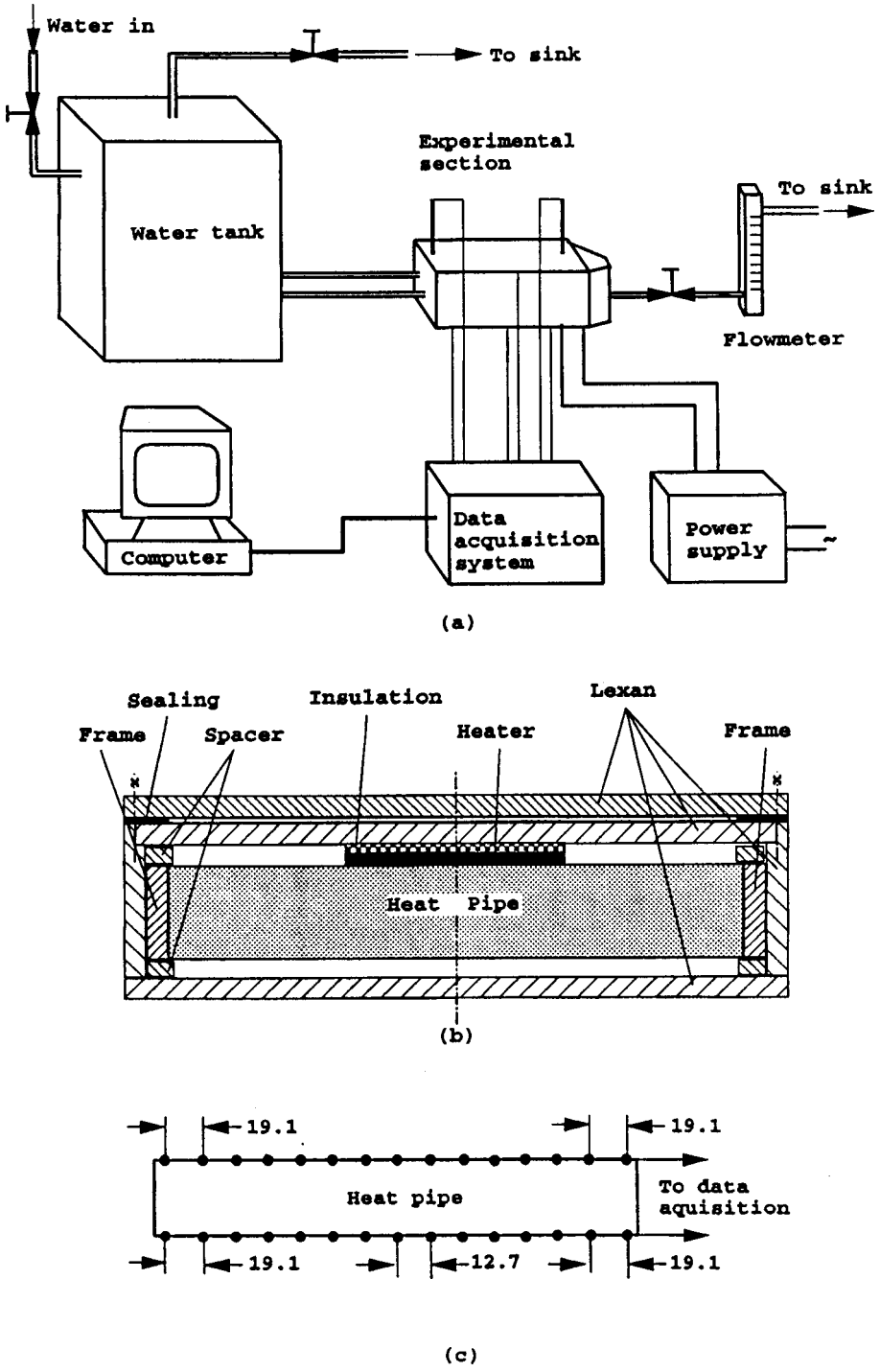

Fig. 2 Experimental setup: (*a*) experimental system, (*b*) cross-sectional view of the channel, (*c*) location of thermocouples on the heat pipe surfaces

ranges. The measured parameters include temperatures on the heat pipe surface, the temperature of the cooling water at inlet and outlet, the flow rate, and the input power. In each experimental run, the average heat transfer coefficient was maintained constant.

Thirty E-type thermocouples were utilized to measure the top and bottom surface temperatures at the centerline of the heat pipe with fifteen on each surface of the heat pipe. In order to reduce the disturbance, a 6-mm by 0.3-mm groove was machined in the heat pipe walls and a high conductivity cement was used to imbed the thermocouples within the heat pipe wall. The spacing between adjacent thermocouples was 12.7 mm, except for the thermocouples at the end, which were separated 19.1 mm from each other, as shown in Fig. 2(*c*).

In order to monitor the heat loss through the insulated surfaces, thermocouples were also installed on both the inner and outer surfaces of the Lexan frame. In addition, two thermocouples were incorporated to monitor the cooling water temperature at the inlet and outlet, and three thermocouples were mounted on the inner surface of the bottom channel wall directly beneath the heat pipe. The room temperature was also measured with two thermo-

couples. The temperature data was collected through a data acquisition system. The temperatures were sampled every second. All data were collected through the data acquisition system.

For a typical experimental run, the flow rate was adjusted to a desired level. After reaching a steady flow rate, a desired heater power was applied. The power supply was turned off when steady-state conditions were achieved. The steady-state conditions were assumed to have been reached when the changes of the maximum temperature reading was less than 0.2°C within at least 90 seconds. Experiments were conducted to investigate the thermal behavior of the heat pipe during startup and shutdown processes. In addition, to analyze the cyclical operation of the heat pipe during startup and shutdown processes, the power was turned back on when initial conditions were achieved after the shutdown process and the procedure described above was repeated.

4 Data Reduction and Uncertainty Analysis

The heat fluxes on the outside surface of the heat pipe were calculated by

$$q_e = \frac{Q}{A_e} \tag{1}$$

where Q is the power supply and A_e the heat transfer area of the evaporator section. The heat transfer coefficient was obtained by

$$h_{\text{conv}} = \frac{Q}{A_c(T_{wa,oc} - T_\infty)} \tag{2}$$

where $T_{wa,oc}$ is the average temperature on the outside condenser surfaces at steady state and T_∞ is the temperature of cooling water, A_c is the heat transfer area of the condenser section, and

$$q_c = h_{\text{conv}}(T_{wa,oc}(t) - T_\infty(t)) \tag{3}$$

where q_c is the heat flux over the entire condenser section. The temperature at the heat pipe wall-wick interface of the evaporator section can be found from

$$T_{ww,e}(t) = T_{wa,oe}(t) - \frac{q_e h_{wa}}{k_{wa}} \tag{4}$$

where $T_{ww,e}(t)$ is the temperature at the wall-wick interface, $T_{wa,oe}(t)$ is the outside wall temperature of the evaporator section and h_{wa} and k_{wa} are the thickness and conductivity of the heat pipe wall. The temperature at the heat pipe wall-wick interface of the condenser section is similarly obtained from

$$T_{ww,c}(t) = T_{wa,oc}(t) + \frac{q_c(t) h_{wa}}{k_{wa}}. \tag{5}$$

It should be noted that Eqs. (4) and (5) provide a linear extrapolation of instantaneous experimental data based on the measured surface temperatures. As such they approximate the thermal storage, which is implicitly built in the measured surface temperature values. It should be noted that the storage terms for all different layers of the flat-plate heat pipe are fully accounted for in the analytical solution. Since the thermal conductivity of the solid wall is relatively high, the following approximation is invoked at the heat pipe wall-wick interface in the evaporator section for extrapolating the data

$$T_{wa,oe}(t) \cong T_{ww,e}(t). \tag{6}$$

Similarly, the following approximation is made at the heat pipe wall-wick interface in the condenser section for extrapolating data:

$$T_{wa,oc}(t) \cong T_{ww,c}(t). \tag{7}$$

An energy balance between the evaporator section and the condenser section yields

$$q_{wv,e}(t) A_e = q_{wv,c}(t) A_c \tag{8}$$

Table 1 Uncertainty in heat transfer coefficient measurements

h_{conv}, W/(m^2°C)	285	500	800	1000	1260
$\epsilon_{h_{\text{conv}}}$	±5.8%	±7.6%	±10.1%	±11.8%	±13.9%

where $q_{wv,e}$ and $q_{wv,c}$ are the heat fluxes at the wick vapor interfaces of the evaporator and condenser section, respectively. Assuming a linear temperature distribution, these heat fluxes can be represented as

$$q_{wv,e}(t) = k_w \frac{T_{ww,e}(t) - T_v(t)}{h_w} \tag{9}$$

$$q_{wv,c}(t) = k_w \frac{T_v(t) - T_{ww,c}(t)}{h_w} \tag{10}$$

where $T_v(t)$ is vapor temperature, and h_w and k_w are the thickness and conductivity of the wick. The conductivity of the wick can be determined by ([1])

$$k_w = k_{\text{eff}} = k_l \left[\frac{k_l + k_s - (1-\varepsilon)(k_l - k_s)}{k_l + k_s + (1-\varepsilon)(k_l - k_s)} \right]. \tag{11}$$

Substituting Eqs. (8) and (9) into (7) yields

$$T_v(t) = \frac{A_e T_{wa,oe}(t) + A_c T_{wa,oc}(t)}{A_e + A_c}. \tag{12}$$

The maximum uncertainty in temperature and power supply readings was ± 0.1°C and ± 3.4 percent, respectively. The uncertainty in the measurement of the thickness of the walls and wicks was ± 0.001 mm while the uncertainty in the measurement of the length, width, and height was about ± 0.01 mm. Using the method of Kline and McClintock [19], the uncertainties in the heat transfer coefficient measurement were determined and are displayed in Table 1. The overall energy balance was also checked and was found to be satisfied well within less than four percent.

5 Results and Discussion

Figure 3 shows the temporal temperature rise for the outside surface of the heat pipe for different input heat fluxes. As expected, the maximum top wall surface temperature increases with an increase in input heat flux. However, an increase in the input heat flux has less of an effect on the bottom surface temperature of the heat pipe since the heat flux at the condenser section is smaller than that of the evaporator section. The time that it takes for the startup operation to reach steady state is almost the same for these four cases, which indicates that input power has an insignificant effect on the startup time over the range considered in this work. The input heat flux-time histories are plotted in Fig. 4 for the four cases shown in Fig. 3. As expected, the heat flux in the condenser section increases with an increase in the input heat flux.

Figure 5 shows the transient temperature rise on the outside wall surface of the heat pipe for different heat transfer coefficients. As shown in Fig. 5, increasing the heat transfer coefficient reduces the wall surface temperatures on both the evaporator and condenser sections. As can be seen in Fig. 5, increasing the heat transfer coefficient reduces the time it takes to reach steady state. The heat flux-time histories for various heat transfer coefficients are plotted in Fig. 6. As can been seen in Fig. 6, for a fixed input power increasing the heat transfer coefficient reduces the time it takes to reach steady-state conditions. For all these figures, the maximum deviation for the relative temperature errors between analytical and experimental results is from 2.4 percent to 7.9 percent.

Figures 3 to 6 show excellent agreement between the measured and the analytical heat flux and temporal temperature distribu-

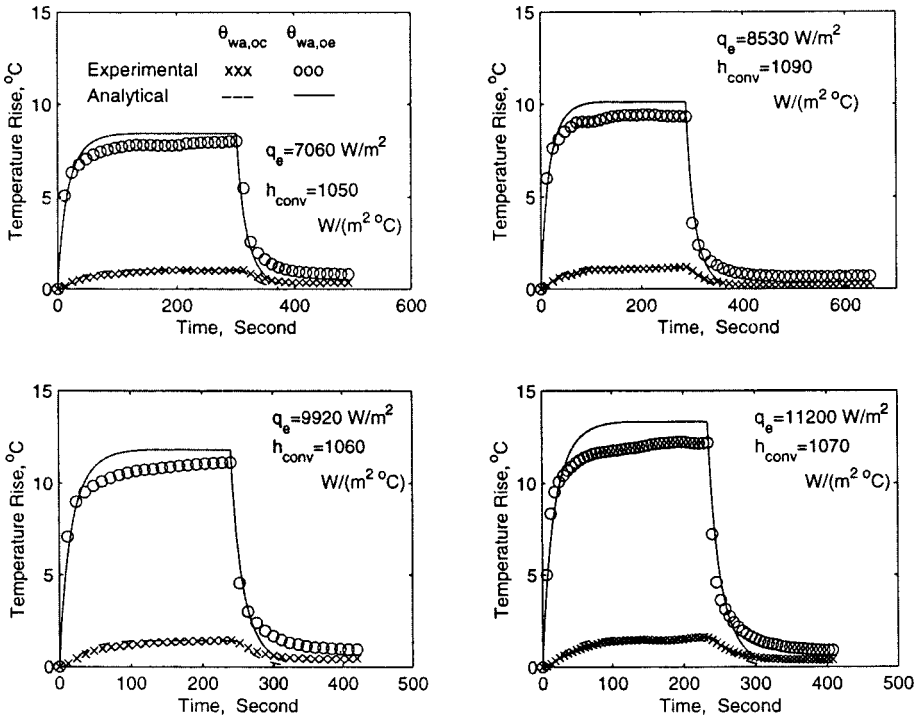

Fig. 3 Temporal temperature rise for the outside surfaces of the heat pipe for different input heat fluxes

tions. As can be seen in Figs. 3 and 5, the measured temperature distributions are a little lower than the analytical temperature distributions under steady-state conditions. This can be attributed to the secondary heat conduction path, i.e., the longitudinal conduction across the top heat pipe wall, which was not considered in the analytical model.

Figures 7 and 8 show the outside surface temperature distributions in the *z* direction for two typical cases. Strictly speaking, the heat transfer along the top wall is two-dimensional, normal as well as along the wall. The heat is predominantly transferred in the normal direction from the evaporator section to the condenser section through the evaporation of working fluid and condensation

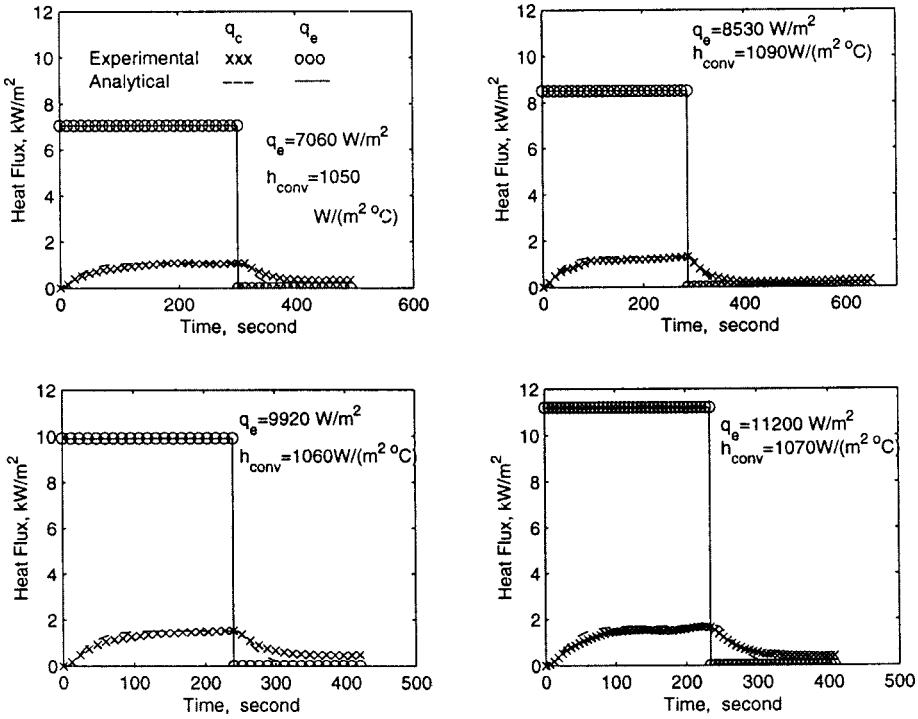

Fig. 4 Heat flux variations for different power inputs

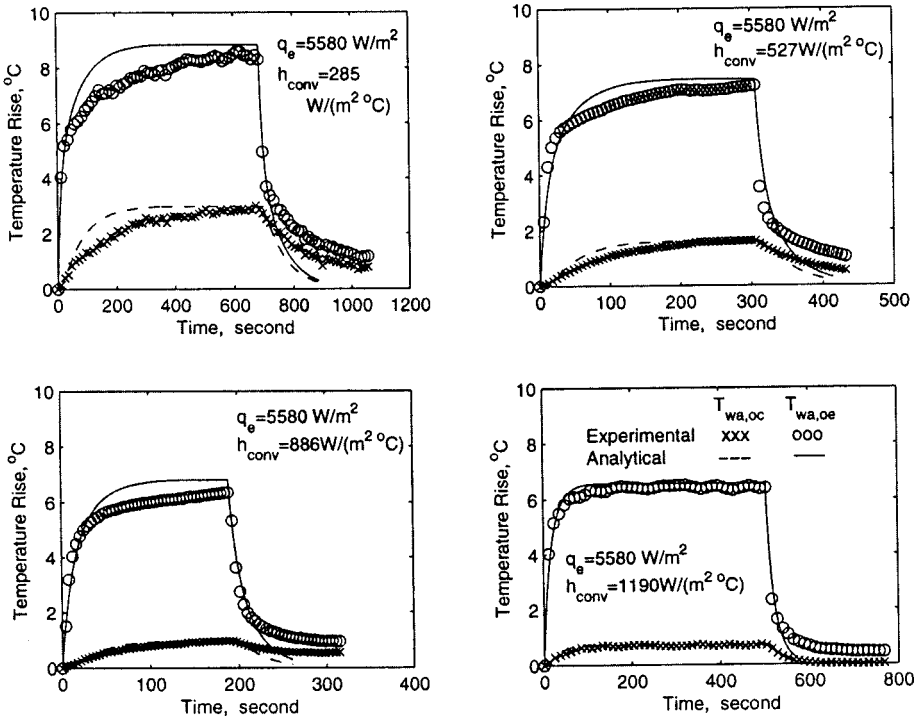

Fig. 5 Temporal temperature rise for the outside wall of the heat pipe for various heat transfer coefficients

of the vapor. The top wall also provides a secondary conduction path for the heat flow in the longitudinal direction. However, this is a relatively minor pathway as evidenced from the good agreement between earlier cited model by Wang and Vafai [6] and the experimental results. Heat transfer through the secondary path can enhance the heat pipe performance by reducing its maximum temperature rise and the maximum temperature difference within the heat pipe.

The transient temperature distributions in the normal direction are plotted in Figs. 9 and 10 for two different input heat fluxes. As

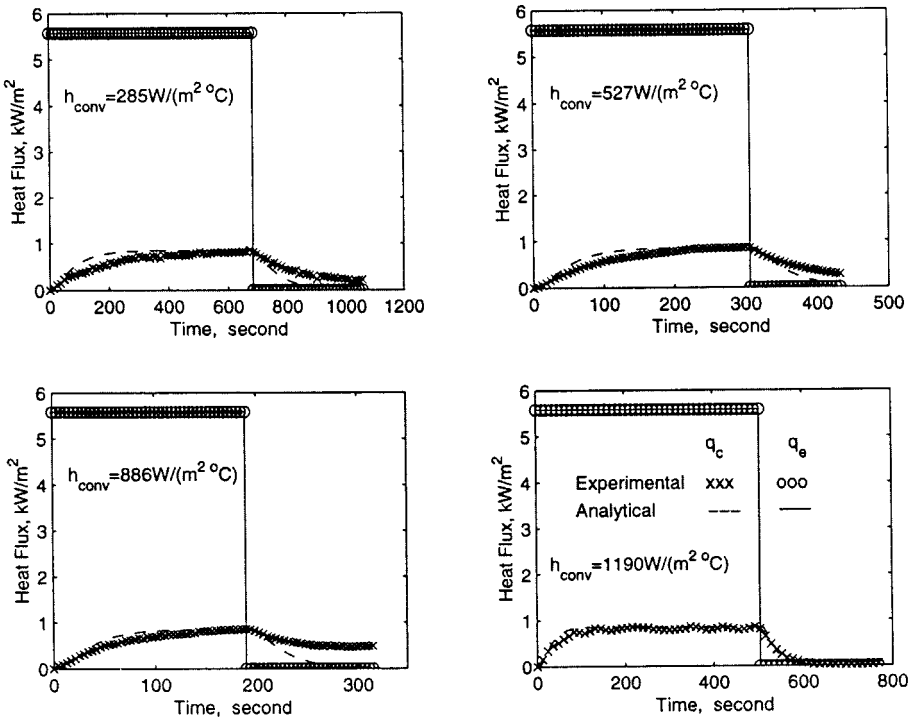

Fig. 6 Effect of heat transfer coefficient variations on the heat flux distribution

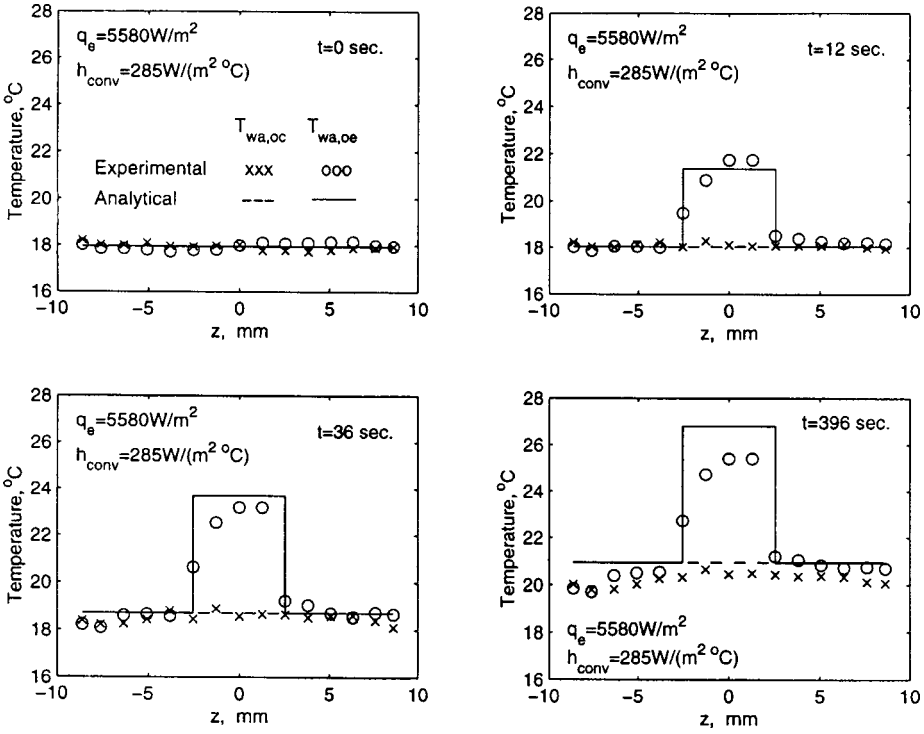

Fig. 7 Temperature distribution along the *z*-direction at different times: q_e=5580 W/m^2, h_{conv}=285 W/(m^2°C)

can be seen in Figs. 9 and 10, the wick in the evaporator section contributes the largest resistance to the total heat transfer. The wick in the condenser section also offers a significant resistance to the total heat transfer resistance. After the power is turned off, the heat pipe tends to have a more uniform temperature distribution as compared to the startup operation.

Figure 11 shows that a decrease in the heat transfer coefficient or an increase in input heat flux results in an increase in the maximum temperature rise. However, the maximum temperature difference within the heat pipe is not sensitive to the changes in

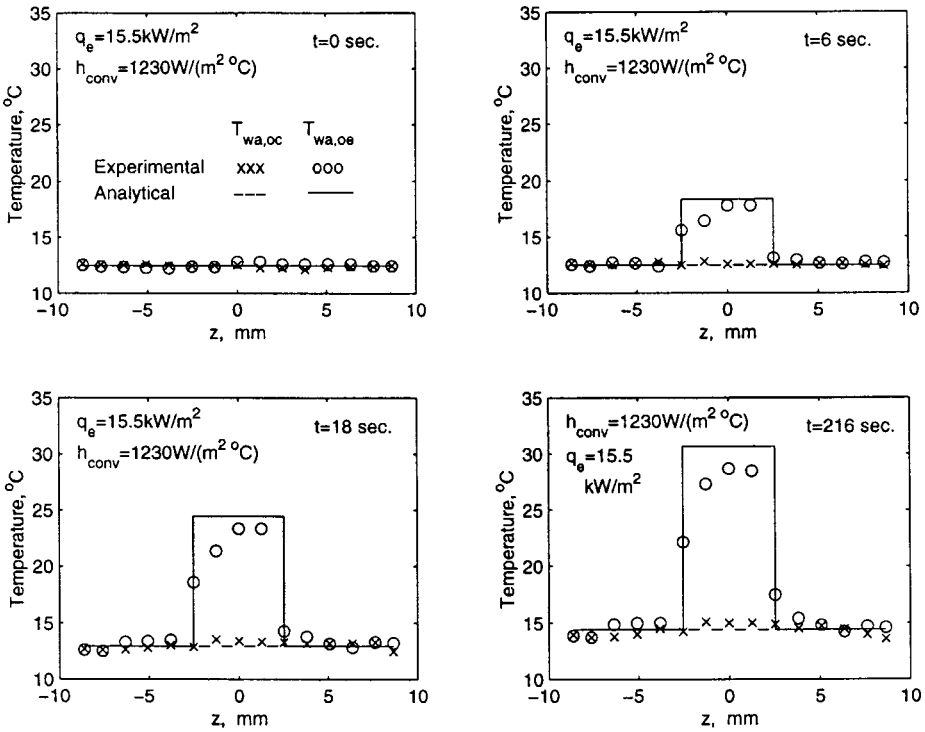

Fig. 8 Temperature distribution along the *z*-direction at different times: q_e =15500 W/m^2, h_{conv}=1230 W/(m^2°C)

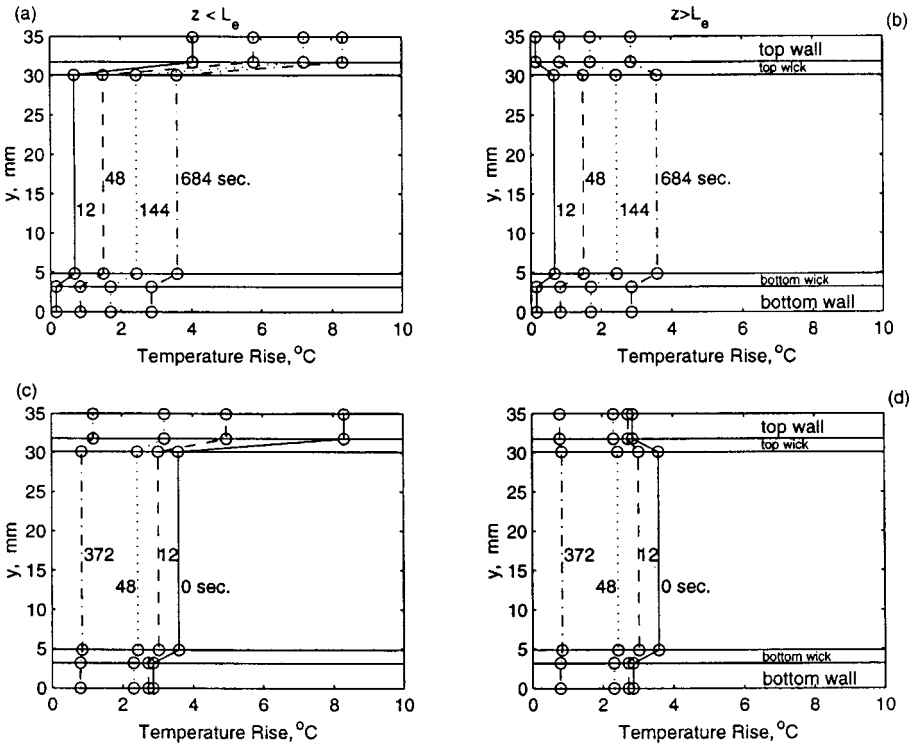

Fig. 9 Transient temperature distribution along the normal direction: $q_e = 5580$ W/m^2, $h_{conv} = 285$ W/(m^2°C)

the heat transfer coefficient. The maximum temperature rise refers to the largest temperature increase on the outside surface of the heat pipe. As can be seen in Fig. 11, variations in the heat transfer coefficient have less of an effect beyond $h_{conv} > 1000$ W/m^2. It can be seen in Fig. 11 that the deviation between the experimental and the analytical results is quite small. However, the deviation increases with an increase in the input power. This maybe attributed to larger contributions of the secondary conduction path for higher input heat fluxes.

Variations of maximum temperature rise in terms of the heat

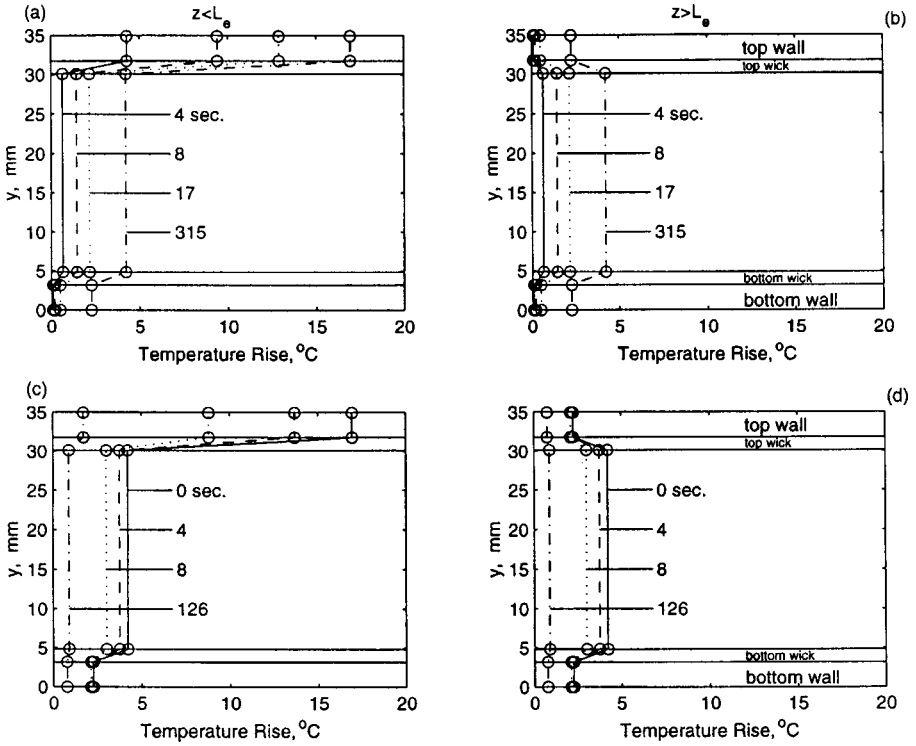

Fig. 10 Transient temperature distribution along the normal direction: $q_e = 15500$ W/m^2, $h_{conv} = 1060$ W/(m^2°C)

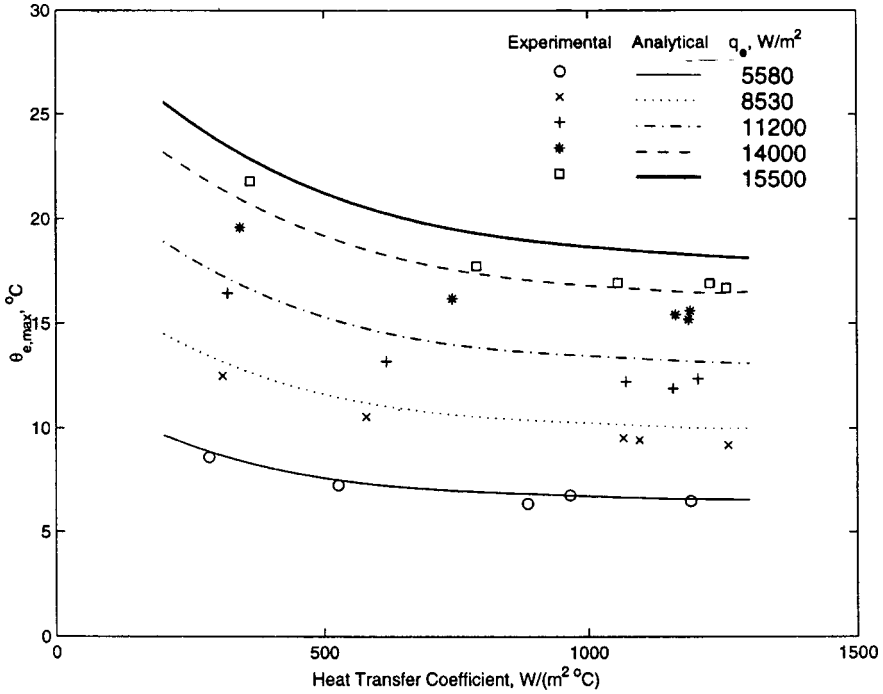

Fig. 11 Effect of variations in heat transfer coefficient and input power on the maximum temperature rise

transfer coefficient and input heat flux can be represented as shown in Fig. 12. This leads to an empirical correlation given below:

$$\theta_{\max}=\left(9.66+\frac{1.57}{h_{\text{conv}}}\right)q_e\times 10^{-4} \tag{13}$$

where

$$5580\ \text{W/m}^2\leqslant q_e\leqslant 15{,}500\ \text{W/m}^2$$

$$285\ \text{W/(m}^2\text{°C)}\leqslant h_{\text{conv}}\leqslant 1260\ \text{W/(m}^2\text{°C)}.$$

In the above equations, q_e is the input heat flux in W/m^2 and h_{conv} is the heat transfer coefficient in W/(m^2°C). The empirical correlation predicts the data with an average error of 1.6 percent. As expected, as in many empirical relationships, Eq. (13) includes system dependent parameters within it. Due to various parameters that are involved in the flat plate heat pipe, more general relationships can be obtained through the use of analytical results presented in Wang and Vafai [6] which have been shown in the present work to be in very good agreement with the experimental results.

Figure 13 displays the maximum temperature difference within the heat pipe as a function of the input heat flux, where this difference refers to the maximum temperature difference on the outside surfaces of the flat plate heat pipe. As shown in Fig. 13, the heat transfer coefficient has an insignificant effect on the maximum temperature difference. The heat input is the main factor, which determines the maximum temperature difference. Figure 13 indicates that the analytical maximum temperature difference is slightly larger than the measured one, which could be attributed to the secondary heat transfer path as discussed previously. Based on Fig. 13, the following correlation can be obtained:

$$\Delta T_{\max}=-0.301+q_e\times 10^{-3},\quad 5580\ \text{W/m}^2<q_e<15{,}500\ \text{W/m}^2 \tag{14}$$

where, q_e is the input heat flux in W/m^2.

Figure 14 shows the time constants for both analytical and experimental results. These time constants are defined as the time it takes for the temperature rise to reach 63.2 percent of its maximum value for a startup operation, and likewise as the time it takes for the temperature rise to drop 63.2 percent for a shutdown operation. As can be seen, there is a very good agreement between the analytical and experimental results. Based on the results given in Fig. 14, the following empirical correlations for the heat pipe time constants for the startup and shutdown operations are obtained:

$$t_{c,up}=35.2-0.0341h_{\text{conv}}1.50\times 10^{-5}h_{\text{conv}}^2,$$
$$285\ \text{W/(m}^2\text{°C)}<h_{\text{conv}}<1260\ \text{W/(m}^2\text{°C)} \tag{15}$$

$$t_{c,\text{down}}=31.7-0.0321h_{\text{conv}}+1.44\times 10^{-5}h_{\text{conv}}^2,$$
$$285\ \text{W/(m}^2\text{°C)}<h_{\text{conv}}<1260\ \text{W/(m}^2\text{SDC)} \tag{16}$$

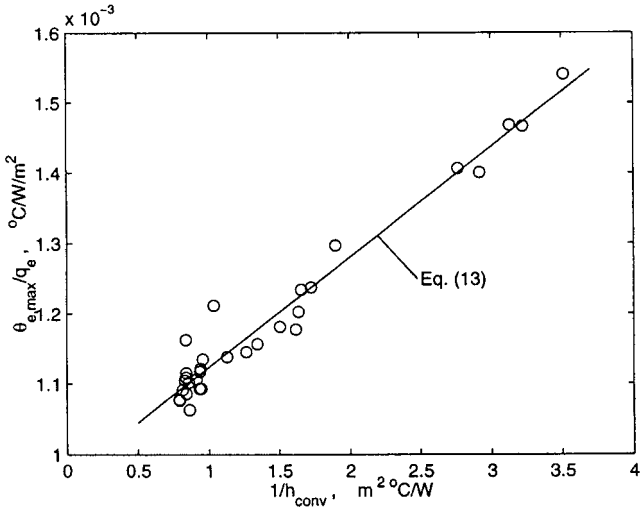

Fig. 12 Compact representation of the maximum temperature rise in terms of the heat transfer coefficient and input heat flux

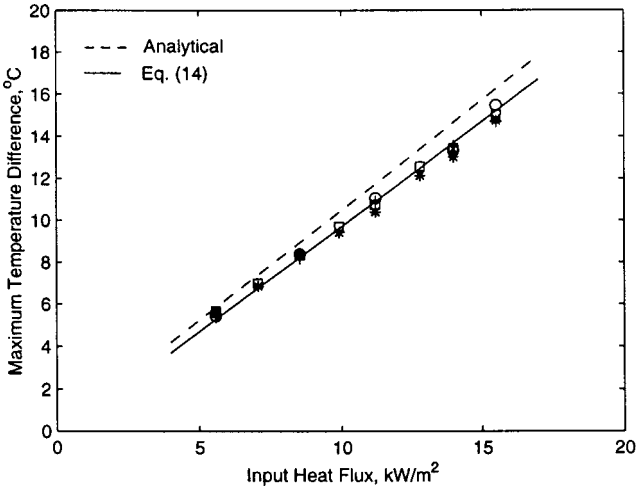

Fig. 13 Effect of input heat flux on the maximum temperature difference

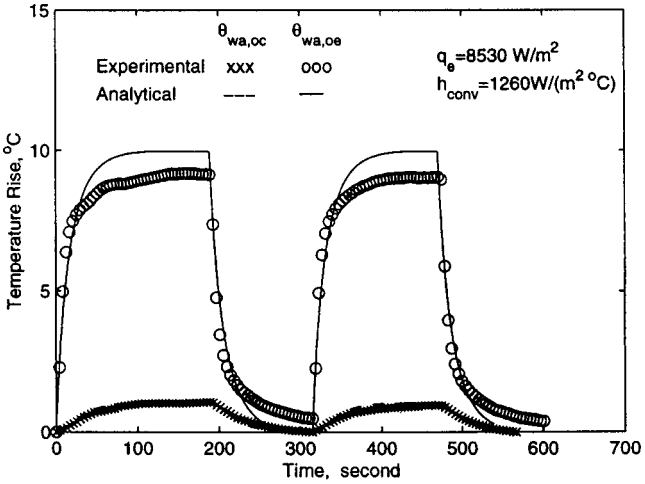

Fig. 16 Temporal temperature distribution for a cyclical operation: q_e=14,000 W/m², h_{conv}=1210 W/(m²°C)

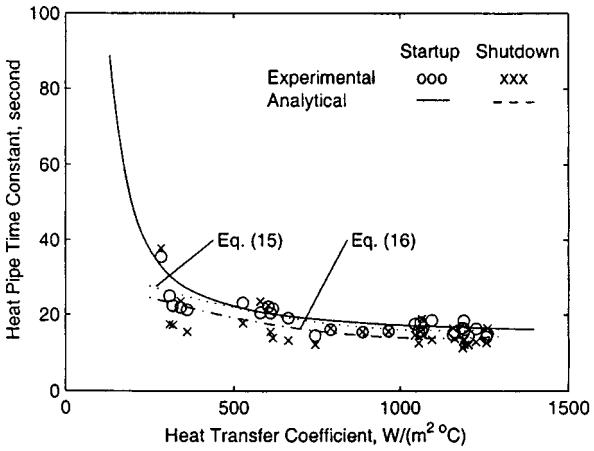

Fig. 14 Time constants for different input heat fluxes for startup and shutdown operations

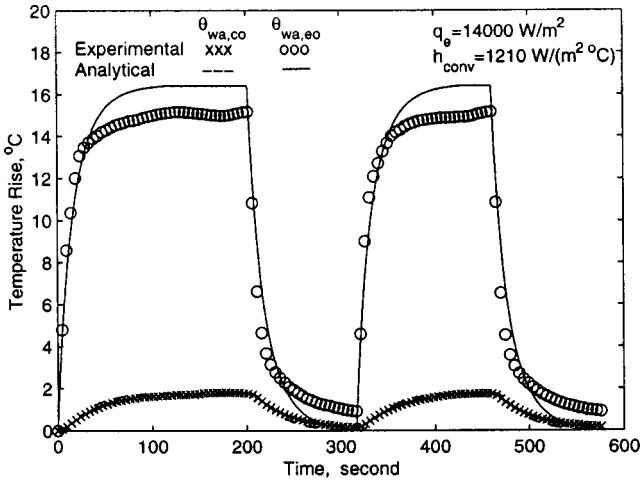

Fig. 15 Temporal temperature distribution for a cyclical operation: q_e=8830 W/m², h_{conv}=1260 W/(m²°C)

where h_{conv} is the heat transfer coefficient in W/(m²°C). Equation (15) predicts the experimental results with an average deviation of 8.4 percent for the startup operation, while Eq. (16) predicts the experimental results with an average deviation of 14.7 percent for the shutdown operation. It should be noted that the four vertical wicks and four edges also affect the time constants.

Figures 15 and 16 show the temporal temperature distributions on the outside surfaces of the heat pipe for a cyclical operation. For the second and the consequent operation cycles, the initial temperature was taken as zero in the analysis, while that was not the case on the experimental side. As shown in Figs. 15 and 16, the initial temperature for the consequent startup operation does not affect the overall performance significantly. Therefore, Eqs. (13)–(16) can be utilized for the startup and shutdown processes during any of the operational cycles.

6 Conclusions

This work presents an analytical and experimental investigation of the thermal performance of a flat-plate heat pipe during startup and shutdown operations. The effects of input power and the heat transfer coefficient on the thermal performance of the heat pipe are investigated. The results show that the wick in the evaporator section provides the largest part of the total thermal resistance, and the wick in the condenser section also contributes a significant part of the total resistance. It is found that the maximum temperature rise increases linearly with input heat flux. For smaller values of the convective heat transfer coefficient (below 500W/(m²°C)), increasing h_{conv} results in a decrease in the maximum temperature rise, while for larger heat transfer coefficients (above 700W/(m²°C)), increasing h_{conv} would have a relatively insignificant effect on the maximum temperature rise.

It was also found that the maximum temperature difference within the heat pipe mainly depends on the input power while variations in the heat transfer coefficient did not have a significant effect. The heat transfer coefficient strongly affects the time it takes to reach steady state while input power has only a slight effect. Empirical correlations for the maximum temperature rise as a function of input heat flux and heat transfer coefficient, and the maximum temperature difference as a function of input heat flux were determined. Correlations were also given for the time constants in terms of heat transfer coefficients. The experimental results for the maximum outside surface temperature rise, maximum temperature difference, heat flux, and time constants were compared with the analytical results and were found to be in very good agreement.

Acknowledgment

The grant (DE-F602-93ER61612) by the Department of Energy is acknowledged and greatly appreciated.

Nomenclature

A = heat input area, m^2
h = thickness, m
h_{conv} = heat transfer coefficient, $W/(m^2°C)$
H = height of the heat pipe, m
k = thermal conductivity, W/(m°C)
q = heat flux, W/m^2
Q = power input rate, W
t = time, seconds
t_c = time constant, seconds
T = temperature, °C
y = normal coordinate
z = normal coordinate
ΔT = temperature difference, °C
ε = porosity
$\varepsilon_{h_{conv}}$ = uncertainty in heat transfer coefficient
θ = temperature rise, °C

Subscript

c = condenser
down = shutdown operation
e = evaporator
eff = effective
l = liquid
max = maximum
oc = outside surface of condenser section
oe = outside surface of evaporator section
s = solid
up = startup operation
v = vapor
w = wick
wa = wall
wv = wick and vapor interface
ww = wall and wick interface
∞ = environment

References

[1] Chi, S. W., 1976, *Heat Pipe Theory and Practice*, Hemisphere, Washington, DC.
[2] Peterson, G. P., 1990, ''Thermal Control of Electronic Equipment and Devices,'' *Advances in Heat Transfer*, Vol. 20, Hartnett, J. P., and Irvine, T. F., Jr., eds., Academic Press, San Diego, CA, pp. 181–314.
[3] Vafai, K., and Wang, W., 1992, ''Analysis of Flow and Heat Transfer Characteristics of an Asymmetrical Flat Plate Heat Pipe,'' Int. J. Heat Mass Transf., **35**, pp. 2087–2099.
[4] Zhu, N., and Vafai, K., 1998, ''Vapor and Liquid Flow in an Asymmetrical Flat Plate Heat Pipe: A Three-Dimensional Analytical and Numerical Investigation,'' Int. J. Heat Mass Transf., **41**, pp. 159–174.
[5] Zhu, N., and Vafai, K., 1998, ''Analytical Modeling of the Startup Characteristics of Asymmetrical Flat Plate and Disk-Shaped Heat Pipes,'' Int. J. Heat Mass Transf., **41**, No. 17, pp. 2619–2637.
[6] Wang, Y., and Vafai, K., 1999, ''Transient Characterization of Flat Plate Heat Pipes During Startup and Shutdown Processes,'' Int. J. Heat Mass Transf., **43**, No. 15, pp. 2641–2655.
[7] Reay, D. A., ed., *Proc. IV Int. Heat Pipe Conference*, Pergamon Press, Oxford, UK.
[8] Basiulis, A., Tanzer, H., and McCabe, S., 1986, ''Thermal Management of High Power PWB'S Through the Use of Heat Pipe Substrates,'' *Proc. 6th Annual International Electronic Packaging Conference*, Int. Electron. Packaging Soc., pp. 501–515.
[9] Thomson, M., Ruel, C., and Donato, M., 1989, ''Characterization of a Flat Plate Heat Pipe for Electronic Cooling in a Space Environment,'' *Heat Transfer in Electronics*, ASME, New York, pp. 59–65.
[10] Bong, T. Y., Ng, K. C., and Bao, H., 1993, ''Thermal Performance of a Flat-Plate Heat-Pipe Collector Array,'' Sol. Energy, **50**, pp. 491–498.
[11] Chen, K. S., Tsai, S. T., and Yang, Y. W., 1994, ''Heat Performance of a Double-Loop Separate-Type Hat Pipe: Measurement Results,'' Energy Convers. Manage., **35**, pp. 1131–1141.
[12] Khrustalev, D., and Faghri, A., 1995, ''Thermal Characteristics of Conventional and Flat Miniature Axially Grooved Heat Pipes,'' ASME J. Heat Transfer, **117**, pp. 1038–1054.
[13] Huang, X. Y., and Liu, C. Y., 1996, ''The Pressure and Velocity Fields in the Wick Structure of a Localized Heated Flat Plate Heat Pipe,'' Int. J. Heat Mass Transf., **39**, pp. 1325–1330.
[14] Khrustalev, D., and Faghri, A., 1996, ''Estimation of the Maximum Heat Flux in the Inverted Meniscus Type Evaporator of a Flat Miniature Heat Pipe,'' Int. J. Heat Mass Transf., **39**, pp. 1899–1909.
[15] Wei, J., Hijikara, K., Takayoshi, I., 1997, ''Fin Efficiency Enhancements Using a Gravity-Assisted Heat Pipe,'' Int. J. Heat Mass Transf., **40**, pp. 1045–1051.
[16] Faghri, A., 1995, *Heat Pipe Science and Technology*, Taylor and Francis, Bristol, PA.
[17] Vafai, K., Zhu, N., and Wang, W., 1995, ''Analysis of Asymmetrical Disk-Shaped and Flat Plate Heat Pipes,'' ASME J. Heat Transfer, **117**, pp. 209–218.
[18] Wang, Y., and Vafai, K., 2000, ''An Experimental Investigation of the Thermal Performance of an Asymmetrical Flat Plate Heat Pipe,'' Int. J. Heat Mass Transf., **43**, No. 15, pp. 2657–2668.
[19] Kline, S. J., and McClintock, F. A., 1953, ''Describing Uncertainties in Single Sample Experiment,'' Mech. Eng. (Am. Soc. Mech. Eng.), **75**, No. 1, pp. 3–8.